UNIVERSITAT POLITÈCNICA DE CATALUNYA

MASTER THESIS

Thermal characterization and stabilization of DFB lasers for access networks

Author:
Roger SOLÉ

Supervisor:
Josep PRAT

A thesis submitted in fulfillment of the requirements for the degree of Master in Electronic Engineering

in the

Grup de Communicacions Òptiques
Departament de Teoria del Senyal i Comunicacions

November 24, 2021

UNIVERSITAT POLITÈCNICA DE CATALUNYA

Abstract

Escola Tècnica Superior d'Enginyeria de Telecomunicació de Barcelona
Departament de Teoria del Senyal i Comunicacions

Master in Electronic Engineering

Thermal characterization and stabilization of DFB lasers for access networks

by Roger SOLÉ

Current optical communication schema are based on TDMA. New schema have been proposed that are based on WDM. A WDM based scheme needs all lasers to be stable at a fixed wavelength. The wavelength of a laser can be modified by temperature changes. In this work, a typical laser used for optical communications is characterized. A thermal-electrical equivalent model is proposed to model the laser. The necessary experiments have been performed to characterize the laser and extract the model parameters. With the model completed, a PI control scheme has been implemented. This implemented control stabilizes the laser to a certain degree but the fabrication and the layout of the packaging prevent a feedback control to have a high performance. Then, a feed-forward control based on measuring the air temperature is implemented. This feed-forward control improves the stability of the laser in front of temperature changes to a satisfactory degree.

Acknowledgements

I would first like to thank my thesis advisor Josep Prat. His expertise on the matter have helped with my development and his advice has been invaluable for this thesis.

I would also like to thank the rest of the members of the laboratory. Their help for the measurements and the analysis of the results. Without their passionate participation and input, the experiments could not have been successfully conducted.

Finally, I must express my very profound gratitude to my family and to friends for providing me with unfailing support and continuous encouragement throughout my years of study and through the process of researching and writing this thesis. This accomplishment would not have been possible without them. Thank you.

Contents

List of Figures

List of Tables

List of Abbreviations

ADC	**A**nalog to **D**igital **C**onverter
DAC	**D**igital to **A**nalog **C**onverter
DFB	**D**istributed **F**eed**B**ack
ECL	**E**xternal **C**avity **L**aser
ESA	**E**lectrical **S**pectrum **A**nalyzer
FTTH	**F**iber **T**o **T**he **H**ome
NTC	**N**egative **T**emperature **C**oefficient
OLT	**O**ptical **L**ine **T**ermination
ONU	**O**ptical **N**etwork **U**nit
PI	**P**roportional **I**integral
TDMA	**T**ime **D**ivision **M**ultiple **A**ccess
TEC	**T**hermo **E**lectric **C**ooler
WDM	**W**avelength **D**ivision **M**ultiplexing

Chapter 1

Introduction

This work is the continuation and analysis of the hardware made by the GCO hardware group for the Versonet project. In that project, the aim is to develop a network for access optical communications based on coherent detection. It had to be compatible with the TDMA scheme used nowadays. The system proposed was based on multiple lasers at different wavelengths (WDM) to make better use of the high spectral capacity of optical fiber.

1.1 Work description and objectives

The current system deployed for optical access communications (FTTH) is called GPON [1]–[3]. It is based on a TDMA scheme. There is one laser for each fiber optic at the central office (OLT) and the same laser with the same data reaches all the end points (homes, ONUs ...). These end points will decode the data from the corresponding time slot previously assigned to them. This scheme, has the advantage that the laser can have any wavelength of the communication band. The main disadvantage of this method is that the only way to increase speed without changing the hardware is to assign a longer time slot to the user. This reduces the time of communication and in turn the speed of the other users.

What is proposed for the new communication system is to have multiple lasers in the same communication band [4]. The distance between two consecutive laser wavelengths has been specified to be 6.25 GHz. This would allow to have up to 256 users in the same band. The bandwidth of the communication has to fall inside the 6.25 GHz slot and leave some margin for possible laser drift with temperature. A scheme similar to the one proposed is currently being used for some network parts such as long haul. However, the standard separation in those cases is 50 GHz. The lasers used will need to have a fixed wavelength as not to interfere with the lasers of other users. The more stable the wavelength is, the faster the communication can be as all the bandwidth can be used.

The main problem to stabilize a laser to a fixed wavelength is the change in temperature. When there is a change in temperature, the laser resonant cavity will dilate. This dilation will change the resonant frequency of the cavity and, in turn, change the central wavelength of the laser.

The aim of this work is to characterize a laser's behaviour in front of temperature changes. Also, a control scheme to stabilize the laser at a given wavelength when there are temperature changes will be proposed. Later, this control scheme will be analysed and improved if it is necessary. We will try and reach a satisfactory stabilization in front of temperature changes with this improved control.

1.2 State of the art

There are instruments that produce laser emission at a very stable wavelength. Some commercial ones reach the limit of quantum fluctuations. A commercial external cavity laser (ECL) laser source can have stabilities of up to 50 MHz. The main drawback of these commercial units is the cost, one unit can cost up to 40,000 €. It is not viable to have this technology at each OLT.

A more cost-effective solution is to control the temperature of the laser with a heat source. This is normally done with a TEC device as it can heat and cool the unit by itself. The problem arises now that controlling the temperature is no easy task. There have been works of complex modeling of the complete thermal system [5]–[9]. These models rely on simulation programs, non-linear functions and accurate description of the laser package internals.

There are also some commercial instruments that stabilize a laser with a TEC. These systems are not cheap enough to implement in a commercial OLT. A simple system has to be created to model and control the lasers if the proposed communication scheme is to be implemented.

1.3 Laser packaging

The lasers used for optical communications are DFB lasers. There are several types of packaging for these lasers. The main package types are Butterfly and TO-CAN. These types of packaging are remarkable for their low cost and small form factor. For an ultra-dense WDM system, the lasers have to be thermally controllable, so all packaging types must include some basic elements. These elements are:

Laser diode: It is the actual source of light.

Peltier device: It is the heating and cooling element. It will produce the changes in temperature.

Temperature monitor: It is usually a NTC thermistor. It will provide a measurement of the internal temperature to control.

These three elements will form the system that we want to control. The actual sizes and distances of the elements will depend on the packaging used. In this work, we have focused on Butterfly packaging. This type of packaging has a big thermoelectric cell compared to the rest of the elements and will have sufficient thermal power to change the laser temperature in any situation. For other types of package, the cell is smaller so the tuning capabilities are more limited. A sketch of the different elements can be seen in Figure 1.1.

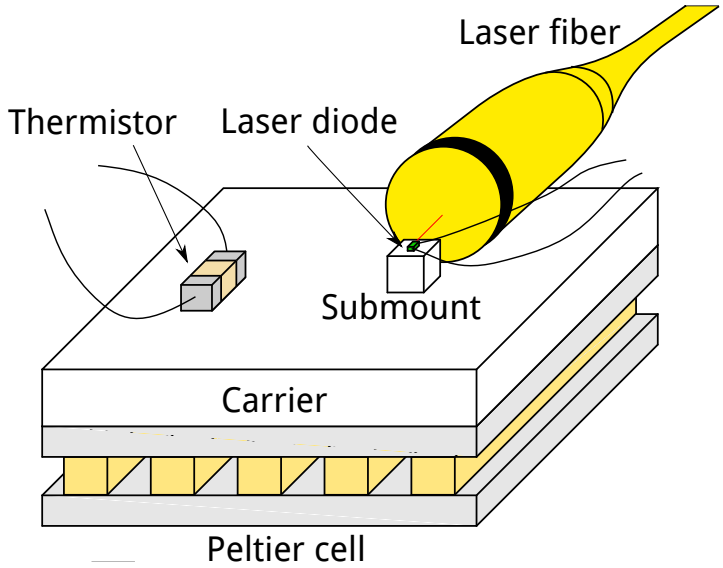

FIGURE 1.1: Physical drawing of the laser inside the package

As seen in the figure, there are also additional elements that have to be taken into account to model the laser. The first one is the carrier plate, a conductor plate that transfers the heat from the Peltier to the thermistor and the laser diode. Another element that has to be taken into account is the laser submount. The laser diode is very small (a few hundred micrometers) and has to be mounted on a heat conducting submount which is as dimensions of a few millimeters. This submount will change the speed of the heat transfer between the laser diode and the other elements. The last element that has to be taken into account is the package itself. It will govern the interactions between all the elements and the outside temperature. These additional elements will vary between different package types even tough they are present in most packaging types.

Chapter 2

Thermal model proposal

In this section a thermal model is proposed. This model takes into account the main interactions from the different elements of the package. It will be based on the thermal-electrical equivalence [10]. We will identify the main interactions and propose a circuital model to match these interactions.

2.1 Interactions

There are two main heat sources in the package. The first one is the Peltier device, and the other one is the laser diode. The laser diode will be heated by Joule effect. This heat will be transferred to the submount and then to the carrier plate. The thermoelectric device has two different thermal effects. The first one is the Peltier effect that creates a temperature difference between the two plates of the device proportional to the current flowing through the element. The other one is the Joule effect. As current will be flowing through the device and it will produce a voltage drop because of the device electrical series resistance, it will suffer Joule heating. The heat from these two effects will be transferred to the carrier plate and then to the other elements.

There is also the interaction between the ambient temperature and each element of the package. This will be determined by the package itself. Also, the Peltier element has a part of conductive heat transfer between both plates.

The last effect that has to be taken into account is the adiabatic chirp of the laser. This effect corresponds to the change in refractive index of the laser cavity when the bias current of the laser changes. As the bias current of the laser change, it will modify the carrier densities in the laser diode. The laser diode also creates the resonant cavity for the laser, so this means that the carrier density in the resonant cavity will change. This change in carrier density will modify the refractive index of the cavity thus modifying the resonant wavelength. This effect is very fast in the order of microseconds and can be considered instantaneous compared to the other ones.

These are the main interactions that will be considered to create the thermal model.

2.2 Complete model

Taking into account the interactions described in section 2.1 we can now create a model of the system. As explained earlier, the model will be based on a thermal-electrical equivalence. The thermal variables have an equivalent as electrical variables as seen in Table 2.1. This method will allow to treat the system with a set of well known tools.

Thermal	Electrical
Heat (Q)	Charge (q)
Heat flow (q_t)	Current (i)
Thermal capacitance (C_t)	Capacitance (C)
Thermal resistance (R_t)	Resistance (R)
Temperature ($^\circ C$)	Voltage (V)

TABLE 2.1: Table with the thermal variables and their equivalent electrical variables

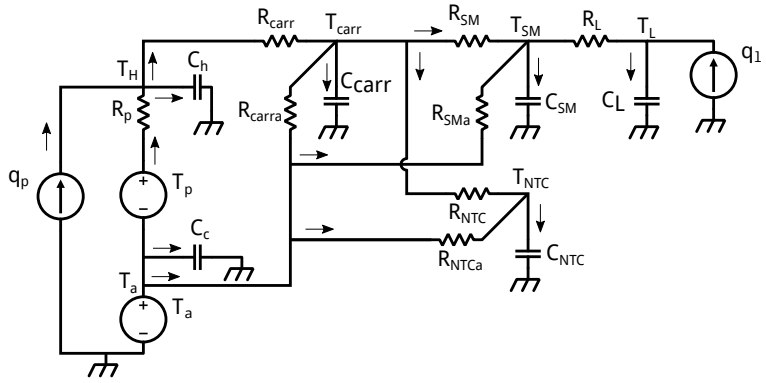

FIGURE 2.1: Proposed equivalent circuit of the thermal model with the thermal-electrical equivalence.

In Figure 2.1 we can see the electrical equivalent circuit proposed taking into account all the interactions previously explained. At the left of the circuit we have the Peltier element. We have followed the general scheme proposed in [11]. It has a heat flow source corresponding to the Joule effect and a temperature difference source corresponding to the Peltier effect. All passive elements are modelled as R-C elements where the resistance models the thermal conductivity and the capacitance the opposition of each element to changing its temperature due to its mass. Following the circuit from left to right, there is the carrier and then the thermistor and laser elements. The thermistor is directly coupled to the carrier plate but the laser chip first has the submount as explained earlier. All elements have the contribution coming from the package that is also modelled as a resistance. The laser chip element also has a heat source that corresponds to the Joule effect heating.

2.3 Model equations

We can apply the Kirchhoff method to solve this circuit. The resulting equations are the following. First there are the 15 voltage equation and then the 6 current equations.

$$q_{cc} = C_c \frac{d}{dt} \mathrm{T_a}\,(t) \tag{2.1}$$

$$q_{ch} = C_h \frac{d}{dt} \mathrm{T_h}\,(t) \tag{2.2}$$

$$R_p q_p - \mathrm{T_a}\,(t) + \mathrm{T_h}\,(t) - \mathrm{T_p}\,(t) = 0 \tag{2.3}$$

$$- R_{carr} q_{carr} - R_p q_p + \mathrm{T_a}\,(t) + \mathrm{T_p}\,(t) - \mathrm{T_{carr}}\,(t) = 0 \tag{2.4}$$

$$-R_p q_p + \mathrm{T_a}(t) - \mathrm{T_h}(t) + \mathrm{T_p}(t) = 0 \tag{2.5}$$

$$-R_{SM} q_{sm} - R_{carr} q_{carr} - R_p q_p + \mathrm{T_a}(t) + \mathrm{T_p}(t) - \mathrm{T_{sm}}(t) = 0 \tag{2.6}$$

$$-R_L q_l - R_{SM} q_{sm} - R_{carr} q_{carr} - R_p q_p + \mathrm{T_a}(t) - \mathrm{T_l}(t) + \mathrm{T_p}(t) = 0 \tag{2.7}$$

$$-R_{NTC} q_{ntc} - R_{carr} q_{carr} - R_p q_p + \mathrm{T_a}(t) + \mathrm{T_p}(t) - \mathrm{T_{ntc}}(t) = 0 \tag{2.8}$$

$$R_{carra} q_{carra} + \mathrm{T_a}(t) - \mathrm{T_{carr}}(t) = 0 \tag{2.9}$$

$$-R_{SMa} q_{sma} + \mathrm{T_a}(t) - \mathrm{T_{sm}}(t) = 0 \tag{2.10}$$

$$-R_{NTCa} q_{ntca} + \mathrm{T_a}(t) - \mathrm{T_{ntc}}(t) = 0 \tag{2.11}$$

$$q_{smc} = C_{SM} \frac{d}{dt} \mathrm{T_{sm}}(t) \tag{2.12}$$

$$q_{carrc} = C_{carr} \frac{d}{dt} \mathrm{T_{carr}}(t) \tag{2.13}$$

$$q_{lc} = C_L \frac{d}{dt} \mathrm{T_l}(t) \tag{2.14}$$

$$q_{ntc} = C_{NTC} \frac{d}{dt} \mathrm{T_{ntc}}(t) \tag{2.15}$$

$$q_p - q_{ch} + \mathrm{Q_p}(t) = q_{carr} \tag{2.16}$$

$$q_{carra} + q_{carr} = q_{carrc} + q_{ntc} + q_{sm} \tag{2.17}$$

$$q_{ntca} + q_{ntc} = q_{ntcc} \tag{2.18}$$

$$q_{sma} + q_{sm} = q_l + q_{smc} \tag{2.19}$$

$$q_l + \mathrm{Q_l}(t) = q_{lc} \tag{2.20}$$

$$\mathrm{q_a}(t) = q_p + q_{carra} + q_{cc} + q_{ntca} + q_{sma} \tag{2.21}$$

As explained earlier, the currents are converted to heat flow and the voltage to temperature. Here, the signs used are that the current (temperature in our case) will flow out of the peltier cell (to the left) and travel to the other devices as indicated by the arrows in Figure 2.1. The naming scheme is the following, q_{carr} is the heat flow across R_{carr}, q_{carra} is the heat flow across R_{carra} and q_{carrc} is the heat flow across the capacitor C_{carr}. So, generalising this naming convention, if the variable has a "a" at the end of the name, the heat flow comes from the ambient temperature and if the variable has a "c" at the end of the name, the heat flow goes across a capacitor. The temperatures of the different components are specified in the schematic.

The result is a third order differential equation that could be solved using the Laplace transform. The resulting equation in Laplace domain is too long to fit in one page, it can be seen in annex A.

2.4 Model reduction

Working with a third order model can come with its pitfalls. This is why the model will be simplified so all the interactions between variables are first order functions. This will leave us with a simplified model that hopefully will also be accurate enough to control the lasers.

The input variables of the laser package are the peltier current, the laser current and the ambient temperature. The output variables are the laser power, the laser wavelength and the thermistor temperature. The simplified model can be reduced

to the one seen in Figure 2.2 where all the interactions can be seen as arrows. All the

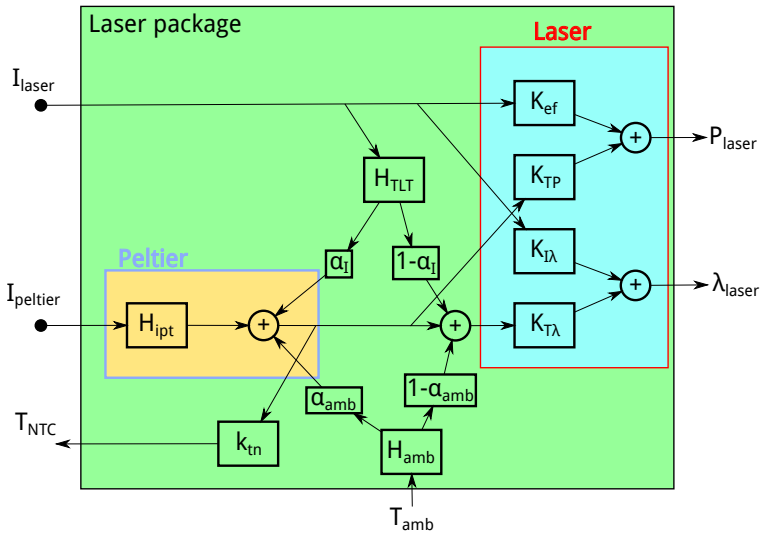

FIGURE 2.2: Block diagramo of the simplified model of the laser with all the main interactions drawn.

transfer functions in this model are first order, this will simplify the controller design and the mathematical calculations. The main interactions are still preserved in this simplified model. The laser chip submount is modelled with the transfer function H_{TLT}, the package temperature interaction is modelled with H_{amb} and also with α_{amb} that will distribute the contribution between the thermistor and the laser diode. The interaction equations with this new model now are the following.

$$\lambda_{laser} = (K_{I,\lambda} + H_{TLT}K_{T,\lambda})\, I_{laser} + (H_{IPT}K_{T,\lambda})\, I_{peltier} + (H_{amb}K_{T,\lambda})\, T_{amb} \tag{2.22}$$

$$T_{NTC} = (H_{TLT}K_{T,NTC}\alpha_I)\, I_{laser} + (H_{IPT}K_{T,NTC})\, I_{peltier} + (H_{amb}K_{T,NTC}\alpha_{amb})\, T_{amb} \tag{2.23}$$

The transfer functions H_{TLT}, H_{IPT} and H_{amb} are a single pole following the expression $H = \frac{k}{\tau s+1}$ where k is the amplification or attenuation and τ is the time constant. So the resulting equations are:

$$H_{TLT} = \frac{k_{TLT}}{\tau_{TLT}s + 1} \tag{2.24}$$

$$H_{IPT} = \frac{k_{IPT}}{\tau_{IPT}s + 1} \tag{2.25}$$

$$H_{amb} = \frac{k_{amb}}{\tau_{amb}s + 1} \tag{2.26}$$

In this work we will not focus on the laser power even though it is important for optical communications. We will assume the laser is biased properly to emit the power needed for the communication. If the laser is modulated by current, the modulation frequency is much larger than the pole frequency of the model equations so the result will be filtered. It is not a problem for our analysis.

In Equation 2.22 there are all the variables that modify the laser wavelength. First we have $K_{I,\lambda}$ that corresponds to the quasi instantaneous adiabatic chirp. Then we

have the change in temperature due to Joule effect of the laser itself modelled by H_{TLT}. The interactions coming from the peltier current, they will create a temperature difference between the laser and the outside temperature. This temperature difference is modelled by H_{IPT}. The package temperature will also affect the temperature of the laser and modify the wavelength and this is modelled by H_{amb}.

Equation 2.23 has the same interactions except the adiabatic chirp. However, in this equation, there is a part of the package temperature and the laser Joule effect that will not affect the thermistor and this is modelled with the α constants that will distribute the contribution between the thermistor and the laser itself. The α constants correspond to the percentage of heat that the thermistor detect over the actual temperature change of the laser.

Chapter 3

Model verification

In this section, the laser will be characterized. The package will be subjected to different tests and from that tests the different parameters corresponding to the model will be extracted. The tests that will be performed are creating a step in the different input variables of the package to find all the time constants and proportional terms of the transfer functions.

3.1 Laser characterization

3.1.1 Measurement techniques

To characterize the laser we have to apply a perturbation to the input and measure the results at the output. To apply the perturbation, a digital to analog converter will be used. For the peltier current perturbation, its output will be fed to a current amplifier and this will provide the current to the peltier cell. For the laser current perturbation, a MOS transistor will be used as a regulator for the current. All the laser bias currents will have the same direction whereas the peltier currents will have to change sign depending on weather the cell is heating or cooling the laser. To apply a step to the package temperature, the room heating will and a freezer will be used.

To measure the different parameters we will use different techniques. The measurement of the wavelength will be done by frequency difference with a stable laser. The scheme can be seen in Figure 3.1.

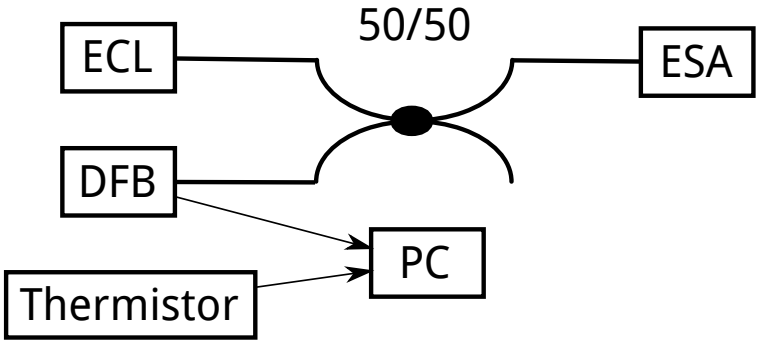

FIGURE 3.1: Wavelength measurement scheme. All the lasers go to a coupler that mixes all the wavelengths and an ESA shows the frequency difference of the wavelengths.

For the stable laser an ECL is used. Its stability is within $\pm 50\ MHz$ regardless of temperature changes within a human comfortable range. This ECL is combined with the laser to measure in a 50-50 coupler. The output of this coupler is then sent

to the ESA. The ESA will display a peak corresponding to the optical frequency difference between the two lasers. The actual measurement we will get is the variation in frequency from the two lasers, assuming the ECL is stable, this variation will correspond to the laser we want to measure. If the wavelength spectrum is observed, the ECL will have a lower wavelength and then the laser that we want to measure will have a higher wavelength. This means that an increase in beat frequency, corresponds to an increase in wavelength. We will follow this convention except when otherwise specified. As we will be applying steps to the input, we are only interested in the variation at the output, so this measurement will suffice to characterize the lasers as we want.

The measurement of the temperature will be taken from the thermistor. The laser temperature can never be known as there is a physical distance between the laser and the sensor but the thermistor will give the best approximation possible. The resistance of the thermistor has to be measured and then using the thermistor equation find the temperature. As all the calculations will be done with an analog circuit, the thermistor will be linearised by this circuit. This circuit will be a voltage divider. It will be composed of a 7.5 $k\Omega$ resistor and the internal thermistor which has a nominal value of 10 Ω at 25 $^{\circ}C$. The voltage reference for the voltage divider will be 5 V. Then, the resulting signal of this voltage divider is conditioned to have a value of 0 V at 30$^{\circ}C$ and a slope of about 8 $^{\circ}C/V \approx 100\ GHz/V$. The temperature measurement of the actual laser chip could also be taken from the wavelength. For a given bias current, the temperature and wavelength will be proportional to each other. In a real control scheme we will not have access to the laser wavelength, so to measure the temperature for the control loop, the only option is the internal thermistor.

There is also an external thermistor to measure the air temperature next to the laser module. It is positioned close to the module, about 10 cm and it is suspended in the air by the connection cables, it is not in contact with any surface. This thermistor is connected to an external temperature monitor that will be connected to a computer. The computer will also be used to measure different signals from the laser PCB through an ADC module.

3.1.2 Peltier TEC characterization

To characterize the laser package we apply a step to the peltier current and measure the different outputs. The step applied will be $\sim 10\ mA$ and it can be seen in Figure 3.2. The bandwidth of the ESA is limited so the step has to be small for the frequency variation to stay in this range. Also, with bigger steps, the system starts to show non linearities that have not been considered in this work.

With this step, the frequency beat and the voltage of the thermistor follow a typical first order response that can be seen in Figure 3.3. As can be seen, there is a drift of the temperature and wavelength in the steady state parts. This is due to the room temperature change. However, this can be compensated by subtracting a line of constant slope to all the points and then the result is a known first order response as seen in Figure 3.4. From these curves we can extract the time constant of each transfer function and the proportional term. By calculating the time it takes to go from 0 to 63% of the final value we can find the value of the time constant. In this case it will be 27.78 seconds. For the efficiency we can see that the step goes from 0.566 mA to $-7.61\ mA$. And the wavelength changes 8.418 GHz. This means that the efficiency of the jump is $k_{IPT} = 1.028\ GHz/mA$.

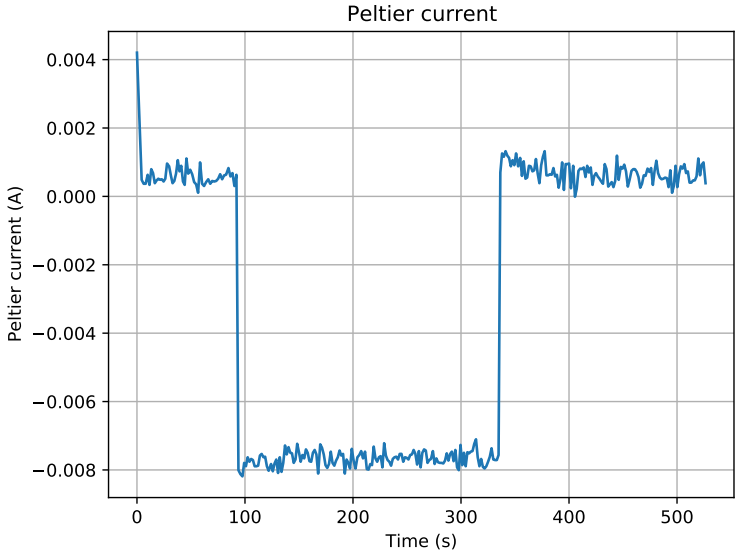

FIGURE 3.2: Current step applied to the peltier for the laser characterization. The step goes from 0.5 mA to 8 mA.

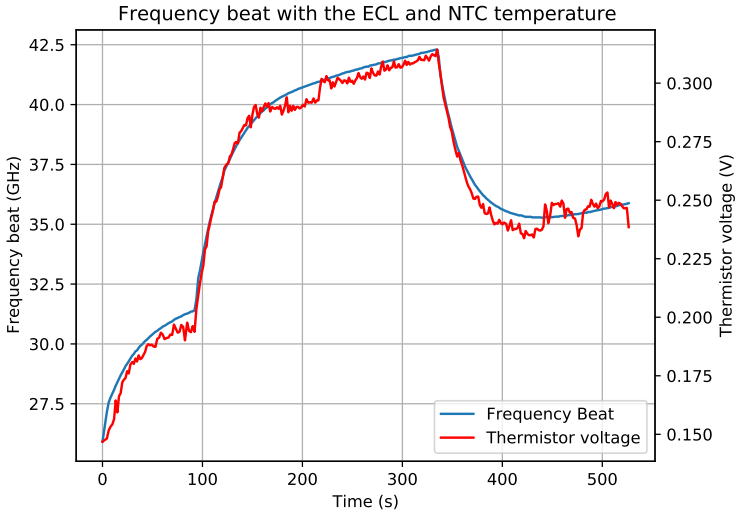

FIGURE 3.3: Response of the frequency beat and the thermistor voltage to the applied step shown in figure 3.3.

3.1.3 Bias current characterization

For the characterization of the laser when the input is the bias current of the chip the method used is the same. A step is applied and the measurements of the frequency beat and the thermistor voltage registered. In this case, the laser current will be stepped between 50 mA and 70 mA. Here, the response will be much faster than with the peltier input so the steps applied are shorter. In Figure 3.5 the applied signal can be seen. This signal produces a first-order-like response to the laser wavelength and the thermistor voltage as seen in Figure 3.6.

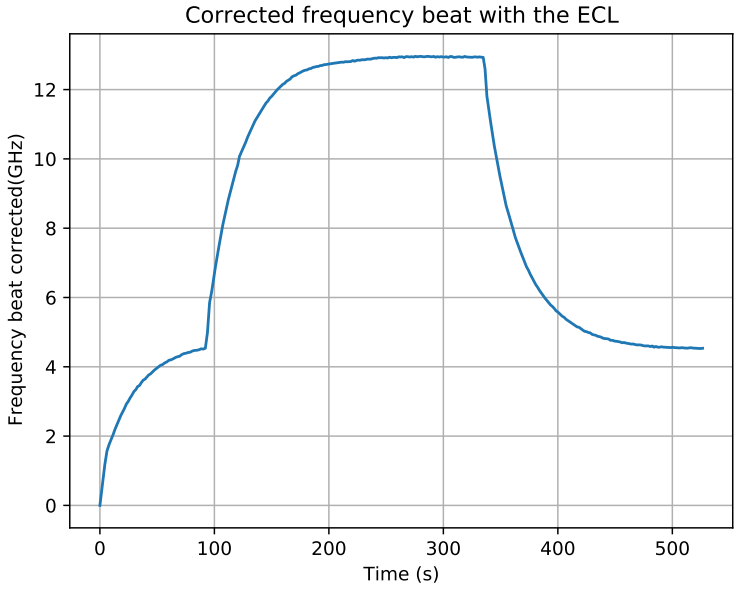

FIGURE 3.4: Corrected response of the frequency beat with the ECL the frequency variation is 8.418 GHz.

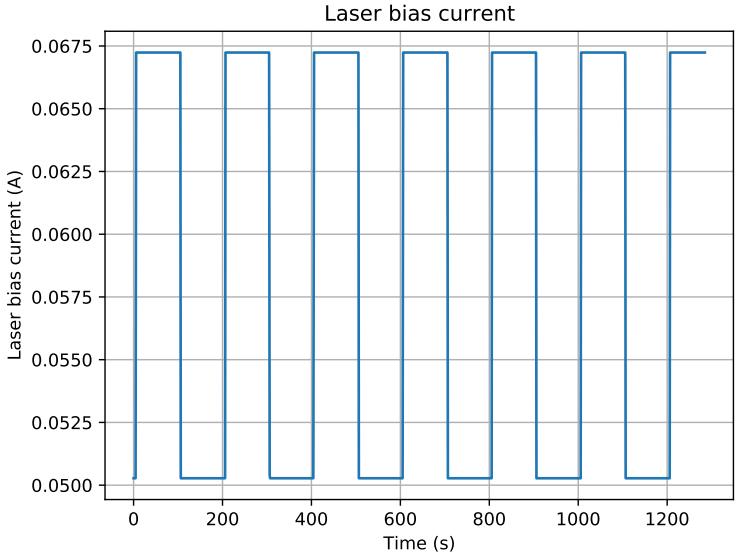

FIGURE 3.5: Current step applied to the laser bias current for the laser characterization. The current step goes from 50 mA to 67 mA. It is a square signal with a period of 200s and a 50% duty cycle.

Even though the pulses applied are much shorter, the wavelength and the thermistor voltage reach steady state. Here we should see a first jump due to the adiabatic chirp and a slow first order response of the Joule heating. It is difficult to appreciate in these graphs. Also, as the bias of the laser is lowered, the emitted power is much smaller, and as the laser changes efficiency with temperature, there are small gaps in the detection where the frequency beat of the ECL and the laser does not have enough power to go over the noise floor of the ESA. That is why there are gaps in the frequency beat curve, there the power dropped under the detectable

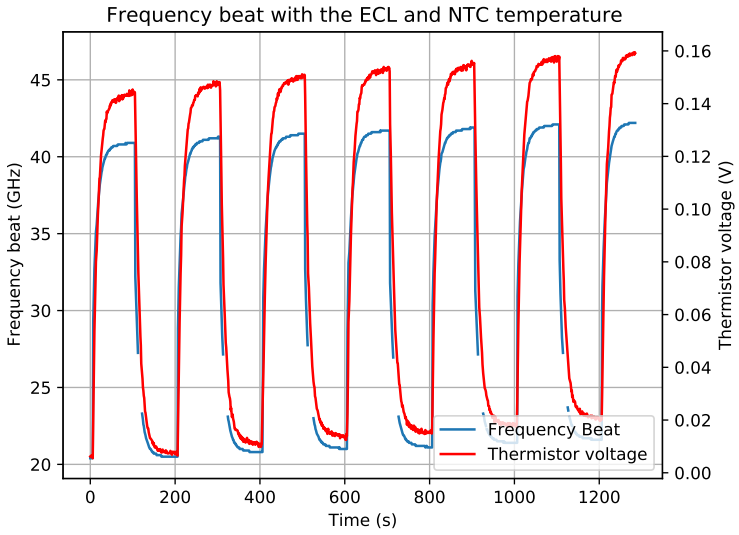

FIGURE 3.6: Response of the frequency beat and the thermistor voltage to the applied step in Figure 3.5.

level. However, it will not pose a problem to extract all the parameters we need to characterize the laser module.

To extract the parameters we need to focus on one of the jumps. In Figure 3.7 the

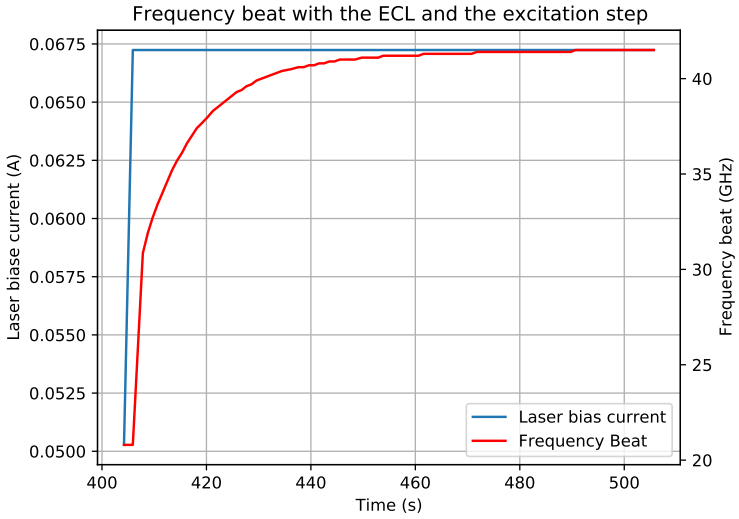

FIGURE 3.7: Single jump when the bias current of the laser changes. Amplified part of the laser bias current and the frequency beat of the lasers.

two effects can be appreciated clearly. First there is a fast jump corresponding to the adiabatic chirp. In this laser, the adiabatic chirp was measured and it has a value of $K_{I,\lambda} = 127\ GHz/A$. Then we have the first order response. The total jump is 11.9 GHz. This means that the total jump is $k = 701.48\ GHz/A$. Taking into account the adiabatic part, the rest is $k_{TLT} = 574\ GHz/A$. The time constant for the thermal part of the jump is $\tau_{TLT} = 10.6\ s$. In this figure there appears to be some delay between the current step and the change in frequency. This is not the case and it is

only an artifact of the discrete sampling time. A single device is used to measure the values and create the step in bias current. Just before the change in bias occurs, the laser is still in the starting wavelength, this corresponds to the first point. The next point corresponds to the change in bias but the measures happen before the change in bias current so the laser has not changed wavelength yet. The next point is when the laser has changed its wavelength and the step takes place.

3.1.4 Ambient temperature characterization

To characterize the package influence against external temperature changes the same method of applying steps has to be applied. In this case, the step to be applied will be an external temperature step. To achieve the step the method used is to insert the laser into a freezer. This will generate a change in temperature. From this change in temperature the frequency variation will be observed. The air temperature is measured with the external thermistor described earlier. The results of this test can be observed in Figure 3.8. In this picture, the frequency corresponds to the actual vari-

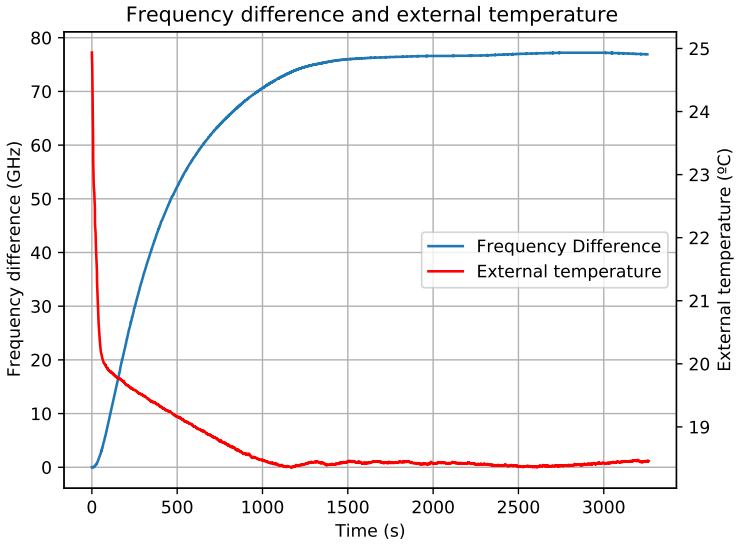

FIGURE 3.8: External temperature and the corresponding frequency of the laser for this step. The internal freezer temperature was set to 18 °C and the room temperature was 25 °C.

ation of absolute frequency, in this case, the wavelength will decrease. As can be seen, the change in temperature is not a perfect step. This is due to the air that escapes when the refrigerator door is opened to put the laser inside it. When the door is closed, the freezer will be able to reach the set temperature but it will take some time. This corresponds to the slope we can see in the temperature line. However, it can still be seen the first order response that was expected for this test. From here the parameters of the model will be extracted.

In this case, as the step is not well-defined, it will not be as straightforward to extract the parameters. Advanced tools of system identification will be used. These tools take an input and an output time curve. Then, try to find the transfer function that will create the output from the input given. Usually, the order of the transfer function is specified by the user. In our case, using this tool, the transfer function found had a proportional term of $k = 4.18\ GHz/°C$ and a time constant of $\tau = 510\ s$.

3.2 Parameter estimation

First, from the datasheet of the laser, it can be obtained that $K_{T,\lambda} = 12.5\ GHz/°C$. Then, with this in mind, the other constants can be found. For the peltier step, the corrected response gave a jump efficiency of $k_{IPT} = 1.028\ GHz/mA$ and dividing by $K_{T,\lambda}$ we get that $k_{IPT} = 82.27°C/A$.

Characterizing the bias current step, from Figure 3.7 we have that $k_{TLT} = 574\ GHz/A = 45.95\ °C/A$.

For the ambient temperature step we got that $k = 4.18\ GHz/°C$. If we want to see how the laser temperature is affected by the external temperature we have to divide by $K_{T,\lambda}$ and the final constant is $k_{amb} = 0.3344\ °C/°C$.

To find the constants to the NTC first the peltier step is used to find the temperature to voltage constant $K_{T,NTC}$. The step from the peltier to the thermistor should be $\frac{V_{NTC}}{I_{peltier}} = \frac{k_{IPT}K_{T,NTC}}{s\tau_{IPT}+1}$. Form the step, the proportional term can be extracted and $k_{IPT}K_{T,NTC} = 10.87\ V/A$ so we get a value of $K_{T,NTC} = 0.132\ V/°C$.

For the α constants, they were defined that the two branches should add to 1 so they would only affect the NTC measurement and not the wavelength. To find α_{amb} the same technique of system identification as k_{amb} is used. In Figure 3.9 the temperature step and the voltage change can be observed. The resulting constant of that algorithm with this step is $k = 0.0411\ V/°C = k_{amb}\alpha_{amb}K_{T,NTC}$. It can be derived from Equation 2.23 that when all other parameters are constant, $T_{NTC} = k_{amb}K_{T,NTC}\alpha_{amb}$. From here, we can find that $\alpha_{amb} = 0.9323$. This means that from the ambient temperature, the thermistor senses 93% of the contribution and the remaining 7% just modifies the wavelength of the laser. Following the same method for α_I, we find that $\alpha_I = 0.8446$. In Table 3.1 we have all the parameters and their values.

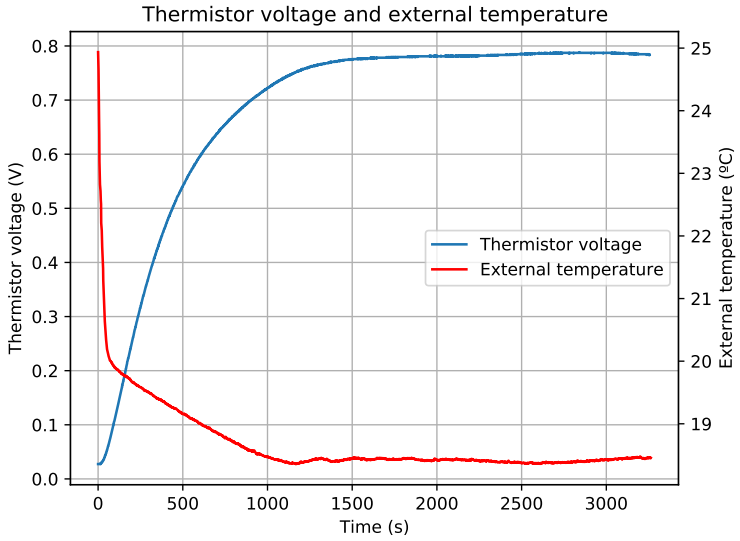

FIGURE 3.9: External temperature step and thermistor voltage when the laser is introduced into the refrigerator. The same as Figure 3.8 but with the thermistor voltage.

Parameter	Value
τ_{TLT}	10.6 s
k_{TLT}	45.95 $^{\circ}C/A$
τ_{IPT}	27.78 s
k_{IPT}	82.27 $^{\circ}C/A$
τ_{amb}	510 s
k_{amb}	0.3344 $^{\circ}C_{las}/^{\circ}C_{amb}$
$K_{I,\lambda}$	127 GHz/A
$K_{T,\lambda}$	12.5 $GHz/^{\circ}C$
$K_{T,NTC}$	0.132 $V/^{\circ}C$
α_I	0.8446
α_{amb}	0.9323

TABLE 3.1: Table with all the model parameters and the value extracted from the tests for one laser.

In the lab there are different laser modules. The techniques described here are the general procedure to characterize each module. Each module will have very different coefficients. For example, the peltier time constant τ_{IPT} has been calculated for all the lasers in the lab. The results are shown in table 3.2.

Laser	Alcatel 4	Samsung 5	Lucent 8	Alcatel 6	Alcatel 7	Lucent 1
τ_{IPT}	27.78 s	13.93 s	9.09 s	22.41 s	30.09 s	8.30 s

TABLE 3.2: Peltier time constant for different laser modules.

Chapter 4

Control scheme

In this section a control scheme is proposed. Then, it will be implemented to control an actual laser module. Finally, the system will be verified. For the verification, two types of tests will be performed. First, a long term stability test. The module will be left subject to room temperature changes and it will have to hold the wavelength of the laser stable. Second, a stress test where the laser will be subjected to a rapid temperature change. For this one, the laser will be inserted into the freezer and taken out to perform the temperature step. In this test the response of the system will be seen as well as the steady state drift.

4.1 Control system proposed and implementation

The control system that will be proposed is a simple PI control. This scheme has been chosen for its simplicity and robustness towards instabilities. The control will be performed from the peltier input leaving the laser bias input to a constant value. The equation of a proportional integral control is the following:

$$C(s) = P + \frac{I}{s} = \frac{Ps + I}{s} = I\frac{\frac{P}{I}s + 1}{s} \tag{4.1}$$

To implement the PI control system the simplest circuit will be chosen. It can be seen in Figure 4.1. This simple circuit was chosen because of its simplicity. Other

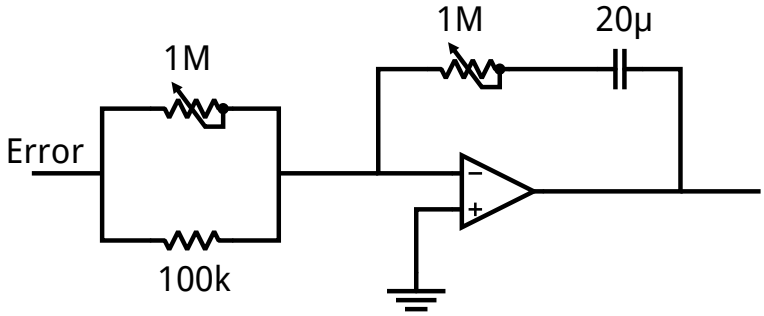

FIGURE 4.1: Circuit schematic of the PI system implemented

circuits have the proportional and integral branches separated and an adder is used at the end to combine the results. It was decided that the capacitor should have a fixed value of $C = 20\ \mu F$ as it is the maximum practical bipolar capacitance available. The input and feedback resistances will be implemented with potentiometers. This is done to allow for the tunability of the PI control when the system is implemented.

This circuit can be analysed as a simple operational amplifier. The gain of an inverting amplifier is

$$A_v = \frac{Z_f}{R_i} \tag{4.2}$$

where Z_f is the feedback impedance and R_i is the input resistance. It is also known that a capacitor in Laplace space has a transfer function of

$$H(s) = \frac{1}{sC} \tag{4.3}$$

This capacitor is in series with R_2 so it can be added as a series impedance.

$$Z_f = R_2 + \frac{1}{sC} \tag{4.4}$$

From Equation 4.2, Equation 4.4 and Equation 4.1 it follows that

$$C(s) = \frac{R_2 + \frac{1}{sC}}{R_1} = \frac{R_2}{R_1} + \frac{1}{sCR_1} = P + \frac{I}{s} \tag{4.5}$$

In the previous analysis, the signs have been ignored as they are not relevant for our purposes.

A tuning process had previously been performed to find proper values of the potentiometers for our application. A step input was introduced to the reference of the control loop and the parameters where tuned to find the fastest response possible with minimum overshoot. Some overshoot could be tolerated as the frequency bands are a frequency range. After the tuning process, the values obtained of the resistances are measured. The two parallel resistances have a value of $R_1 = 90.4\ k\Omega$. The other potentiometer has a value of $R_2 = 503\ k\Omega$. Having all the parameters of the control system now we can find the values obtained. From Equation 4.5 it is easy to see that $P = \frac{R_2}{R_1}$ and $I = \frac{1}{R_1 C}$. In our case, the system has a $P = 5.65$ and $I = 0.55$. The final equation is

$$C(s) = 5.65 + \frac{0.55}{s} = 0.55\frac{10.06s + 1}{s} \tag{4.6}$$

The block diagram of the complete system with the feedback and the control equation can be seen in Figure 4.2. From here we can find the closed loop equation

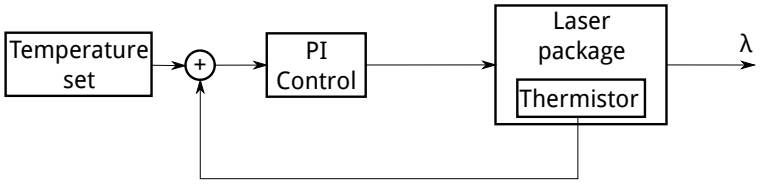

FIGURE 4.2: Complete system with the control equation and the feedback loop. The laser package block is the one shown i Figure 2.2. The input is $I_{peltier}$ and the output is T_{NTC}.

to be

$$H_{CL}(s) = \frac{C(s)H_{IPT}K_{T,\lambda}}{1 + C(s)H_{IPT}K_{T,NTC}} = \\ = 20.2\frac{10.06s + 1}{s^2 + 2.181s + 0.2133} = \\ = 94.69\frac{10.06s + 1}{(0.48s + 1)(9.74s + 1)} \quad (4.7)$$

We can see from this that the pole and zero are very close to each other. One simplification that could be made is to cancel the zero and pole to have a first-order system.

4.2 Result verification

As explained earlier, two types of test will be performed to verify the effectiveness of the control scheme implemented. The first one is to keep the laser inside the freezer and switch the freezer on and off in a periodic interval. This will enable us to create a repeatable test scenario where the results can be compared. The temperature change and the frequency drift can be seen in Figure 4.3. From this figure, some first

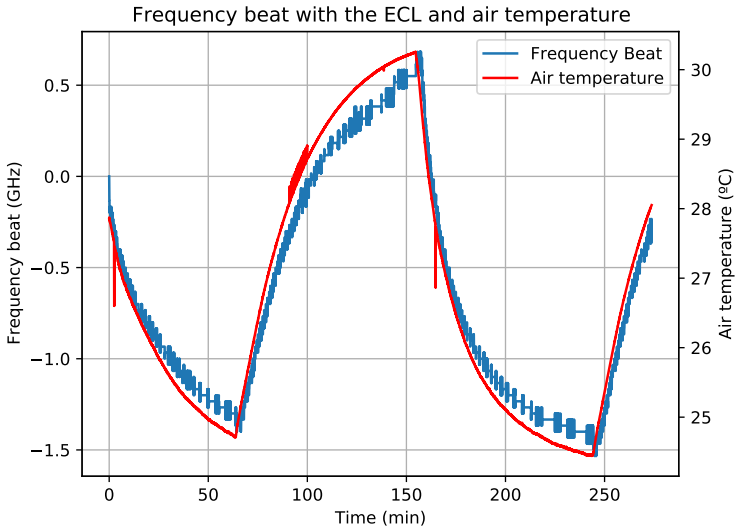

FIGURE 4.3: Frequency beat of the ECL and DFB when the laser is in the refrigerator and the air temperature. The refrigerator is being switched on and off with a period of 3 hours.

conclusions can be extracted. The temperature changes from 25 $^{\circ}C$ to 30 $^{\circ}C$. The frequency has a drift of 2 GHz for this temperature change. This equates to a drift with temperature of 381 $MHz/^{\circ}C$. This drift can come from many effects. Other signals of the control loop have to be observed to find the origin of this drift. In Figure 4.4 the internal thermistor voltage, the loop reference voltage and the loop error can be seen. Here, different effects can be seen. The thermistor voltage has the expected response when a perturbation is applied to the loop. When there is a change in external temperature, there is a deviation from the reference voltage and then it slowly converges to the reference. The error signal has been filtered by a moving average of 10 samples. It has a typical response of an error in a control loop. The

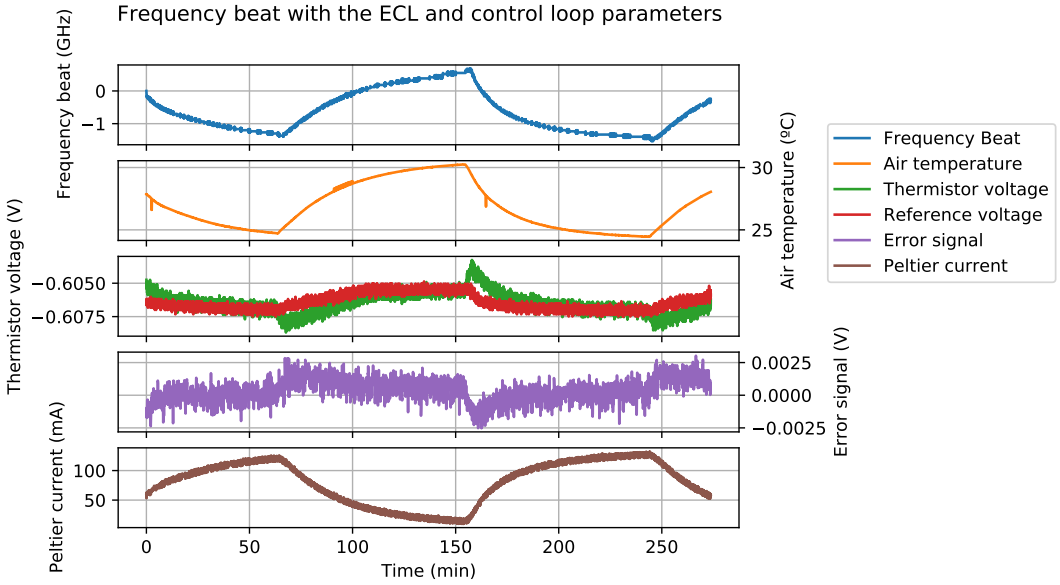

FIGURE 4.4: Different parameters of the control loop when the laser is in the refrigerator.

error increases when there are the perturbations to the external temperature, this is expected in a normal control loop. The error converges to zero after some time. This is to be expected as the loop is working properly. If the reference voltage is observed, some drift can be seen. The reference should be stable, especially with temperature. In our case, this variation of reference comes from a bad design of the circuit. A voltage reference was used but it was not properly biased. This could be one source of the error seen in frequency. Using Equation 4.7 it can be seen that this difference in voltage reference of 0.0012 V corresponds to 113 MHz of frequency drift. For this temperature difference this corresponds to 19.53 $MHz/°C$. From the total frequency drift, this is a very small amount. It can be noticeable if the temperature changes are big and should be corrected but it is not the main effect of the temperature drift seen. The other possible effect to introduce a frequency drift is the difference in temperature between the NTC and the laser. In Table 3.1, it is specified that the percentage of air temperature variation that the thermistor senses i 93.23 %. This means that the 6.77 % of the variation will not be corrected by the control loop. Using the other parameters from the table, it can be found that this will account for 282.6 $MHz/°C$. This contribution is much more important than the previously calculated and corresponds to the majority of the drift. Apart from these two effects, there will also be second order effects and non linearities that this derivation and control will not take into account. Unfortunately, even if the control scheme is perfect and the reference has no drift with temperature, the best drift that can be achieved is 282.6 $MHz/°C$.

The second test is to create a step in air temperature. The results of this test are in Figure 4.5. Here, there are two jumps in temperature, a first one from room temperature to inside the refrigerator and another one from the refrigerator to the room temperature. The first one is from 28 $°C$ to 21 $°C$. The second one goes from 21 $°C$ to 28 $°C$. Controlling the room temperature is a challenging task so when the laser is outside the refrigerator, the temperature changes over time. However, it does not affect the results that can be extracted. It can be seen that when there is a change in temperature, there is a fast counter jump in wavelength. There is also the slow

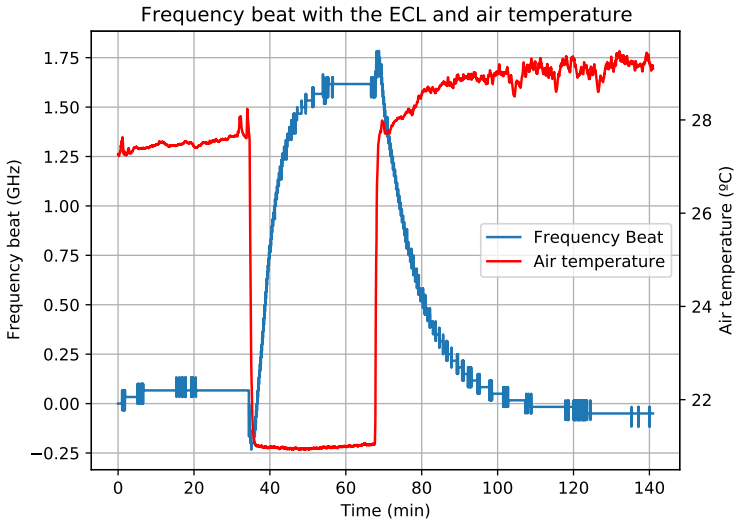

FIGURE 4.5: Frequency beat of the ECL and DFB when a step in air temperature is performed.

drift that corresponds to the effect explained earlier. A part of the temperature variation will not be sensed by the thermistor so the control loop cannot correct it. This fast counter jump can be due to the control loop not being fast enough to keep up with such a fast change in temperature. The temperature change is a perturbation and the control loop will take some time to react and correct this perturbation. During the time it takes, the wavelength of the laser will experience a small drift and this small drift is what can be seen in this plot. It can be perfectly appreciated in both jumps. We can calculate the magitude of this counter jumps. In this case, it is 50.14 $MHz/°C$.

4.3 Ambient temperature compensation

A problem that comes to light with the current control system is the inability to measure the actual laser temperature. To circumvent this problem, there are several methods that can be used. The laser is a diode emitter. As all diodes, the I-V curve will change with temperature. If we are able to measure the current and voltage across the laser, we could find the position in the I-V curve. If the curve is well-defined for different temperatures, the actual temperature of the laser can be found. This would be an instantaneous method of measuring the laser temperature. The problem with this method is that the laser has to be characterized with temperature to find the relation between the I-V curve and the temperature. The other problem is that it would probably require a lookup table. This means that this method can only be used with a digital control scheme. Another solution that could solve the same problem is to add a thermistor that measures the air temperature close to the laser. With this new thermistor, the air temperature can be sensed and a correction introduced to the reference voltage of the loop. This would be a small correction that should not affect the tunability of the laser. It can also be added a fast compensation that reduces the fast counter jump at the start of the temperature change. This addition could be done with an analog system and added to the current system. Now, this second solution will be implemented.

In essence, it will be a feed forward system that measures the ambient temperature and applies a compensation to the voltage reference. We want to compensate the drift in temperature when the ambient temperature changes. The transfer function going from the ambient temperature to the wavelength is in equation 4.8 and it can be extracted from Figure 4.6.

$$\frac{\lambda(s)}{T_{amb}(s)} = H_{amb}\left(\frac{1}{1+C(s)H_{IPT}K_{T,NTC}}\alpha_{amb} + (1-\alpha_{amb})\right)K_{T,\lambda} \tag{4.8}$$

The transfer function from the loop reference is Equation 4.7. With these two equa-

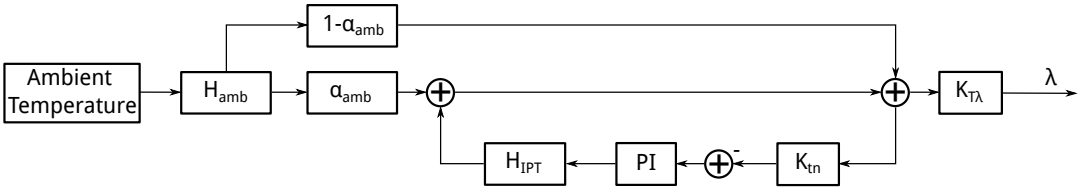

FIGURE 4.6: Feedback system from the ambient temperature input $\frac{\lambda(s)}{T_{amb}(s)}$.

tions the compensation scheme can be built. The control scheme can be seen in Figure 4.7. We want to obtain that with a change in air temperature, the wavelength

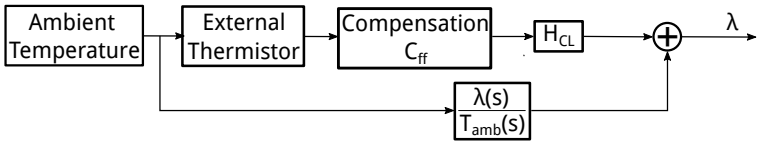

FIGURE 4.7: Block diagram of the feed-forward system implemented for the ambient temperature compensation. H_{CL} corresponds to the complete closed loop equation coming from the reference voltage shown in Figure 4.2 and $\frac{\lambda(s)}{T_{amb}(s)}$ corresponds to the closed loop equation coming from the ambient temperature. The compensation block is the one designed.

stays fixed. To accomplish this, we have to find the compensation transfer function.

$$\frac{\lambda(s)}{T_{amb}(s)} = C_{ff}H_{CL} + \frac{\lambda(s)}{T_{amb}} = 0 \tag{4.9}$$

Where C_{ff} is the compensation block we want to design. To accomplish this, we need that

$$C_{ff}(s) = -\frac{\lambda(s)}{T_{amb}}\frac{1}{H_{CL}} = \\ \frac{k_{amb}\left(\alpha_{amb}s\left(\tau_{IPT}s+1\right)+\left(\alpha_{amb}-1\right)\left(K_{T,NTC}k_{IPT}\left(I+Ps\right)+s\left(\tau_{IPT}s+1\right)\right)\right)}{k_{IPT}\left(I+Ps\right)\left(\tau_{amb}s+1\right)} \tag{4.10}$$

Where we used Equation 4.7, Equation 4.8 and Equation 4.9 to find the values of the control equation. All the values are the ones found in table 3.1 and R_1, R_2 and C_{pi}

are the values of the PI control circuit. Substituting the values we get

$$C_{ff}(s) = -\frac{\lambda(s)}{T_{amb}}\frac{1}{H_{CL}} = \frac{3.46 \cdot 10^{-5}s^2 - 4.62 \cdot 10^{-6}s - 5.82 \cdot 10^{-7}}{s^2 + 0.101s + 1.949 \cdot 10^{-4}} \tag{4.11}$$

We will try and use this compensation function to further stabilize the wavelength in front of temperature changes.

4.3.1 Digital compensation

The first system implemented was a digital control. To implement it we used the external thermistor connected to a computer through an ADC to read the air temperature and a DAC module to modify the set temperature of the control loop and introduce the compensation. The Equation 4.11 was transformed to discrete time and an algorithm implemented to compute the result of the transfer function with a given input for each time sample. This algorithm was implemented in a Matlab environment. Matlab was chosen because it is the most widely used tool in our laboratory and it is easy to use. However, it has a major drawback for this application which is the lack of real-time programming. In Matlab, the timing of the execution cannot be controlled by the user and is dependant of the operating system of the computer. In our setup, we found that the fastest data sampling rate that would reliably perform the computations in a fixed time was of 0.1 samples/s. Meaning that, as we want a fixed time step between samples, the control system is relatively slow.

Even with this problem, the system was implemented to compensate the external temperature variations. The results can be seen in Figure 4.8. It can be seen that the

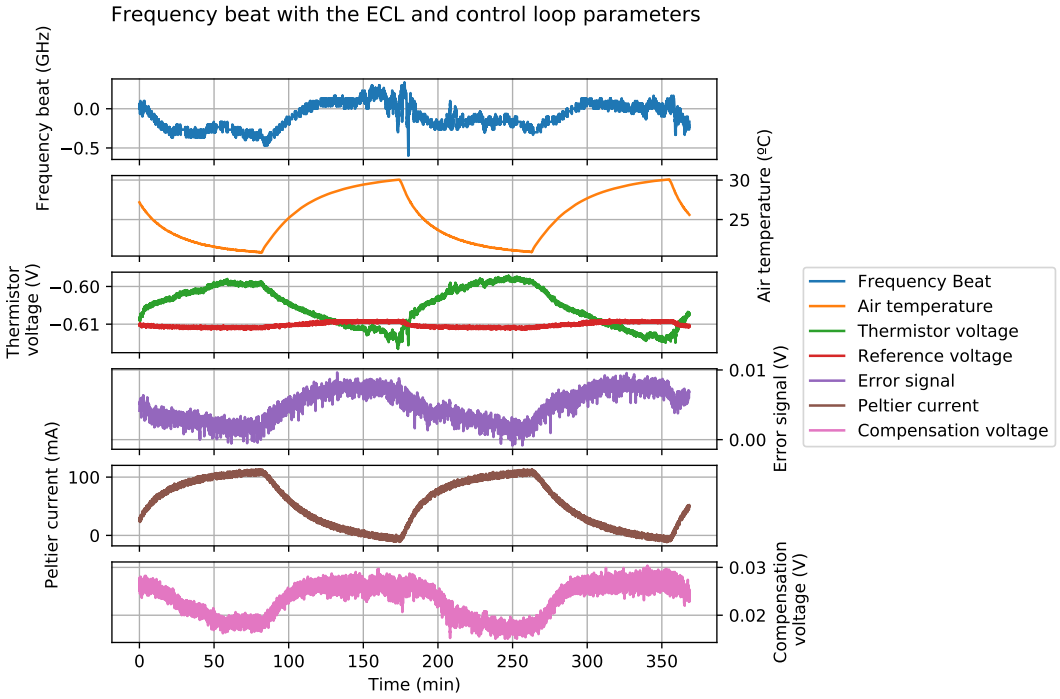

FIGURE 4.8: Different parameters of the control loop when the laser is in the refrigerator with the external thermistor compensation. Same setup as the other tests. The compensation comes from the variation of the loop reference.

variation with temperature has been reduced. It has gone from 381 $MHz/^{\circ}C$ to 100 $MHz/^{\circ}C$. This reduction has broken the barrier of the 283 $MHz/^{\circ}C$ that the internal thermistor imposes and that was explained earlier. Also, we can see that the wavelength does not have the general shape of the air temperature as it happened on the previous tests. In the last graph of the figure the compensation voltage can be seen. This voltage is what modifies the set point of the control loop. That is why the reference voltage and the thermistor voltage (controlled variable) do not have the same value. We would need to add the compensation voltage to the reference voltage. However, the compensation could be improved. We would need to use a faster control system so the discretization does not affect the overall system. This could be implemented digitally with a dedicated system for the control such as a microcontroller with a real-time operating system. Such a device would ensure the proper timing for the compensation function and also make the system much faster.

4.3.2 Analog compensation

As explained earlier, the digital compensation can be improved. Now, instead of using a digital compensation, we use an analog compensation. This will solve the problem of the speed but will introduce new problems that we will have to solve. The general idea of the compensation is the same, the temperature will be measured and based on the measurement, the reference of the loop will be modified. In this case, all the mathematical operations will be performed with an analog system. This system will be a first-order system to keep the simplicity of the system.

When observing the response of the laser to temperature steps in Figure 4.5 we can clearly see two different errors as expected from the theoretical model. A steady state error that makes a drift in frequency for static temperature changes and a transient error that affects the dynamic changes. It can be observed that the two errors have different sign. We can try and extract the response from equation 4.10. For the low-frequency response we substitute s by zero and we get that $C_{ff}(s=0) = K_{T,NTC}k_{amb}\left(\alpha_{amb}-1\right) = 2.9\cdot 10^{-3}$. To calculate this, the values of the parameters in Table 3.1 are used. For the high-frequency response, we substitute s by ∞. Now we have to discard the terms that do not include the ∞ because they will not be significant. We end up with $C_{ff}(s\to\infty) = \frac{k_{amb}(\alpha_{amb}\tau_{IPT}+(\alpha_{amb}-1)\tau_{IPT})}{k_{IPT}P\tau_{amb}} = 3.5\cdot 10^{-5}$. These parameters can also be extracted from the bode diagram of the function. The bode diagram of equation 4.11 is displayed in Figure 4.9. As it can be perceived in the bode diagram, there are also two responses with different signs. First there is a low-pass response with a magnitude of $2.9\cdot 10^{-3}$ and then a high-pass response with a magnitude of $3.4\cdot 10^{-5}$. The sign of the responses can be extracted from the phase. This response is dependent on the laser parameters. We will simplify this response to a first order system with one pole and one zero. The zero has to be in the right-hand plane to have the correct phase change. To do this, we take the high and low frequency magnitudes and try and preserve those. Then, we will create a pole zero pair at the mid-frequency range to go from one magnitude to the other one. In our case, this pair is between 0.02 Hz and 0.03 Hz. These values correspond to a time constant of 50 s and 33.33 s. When the PI control was designed, the parameters were tuned for the fastest jump possible allowing for some overshoot. Equation 4.7 shows the closed loop equation. We can see that the pole and the zero almost cancel out. We can force the PI system to exactly cancel the pole introduced by the Peltier device. This can be done by making the capacitance of the PI $C_{PI} = \frac{\tau IPT}{R_2}$. If we do

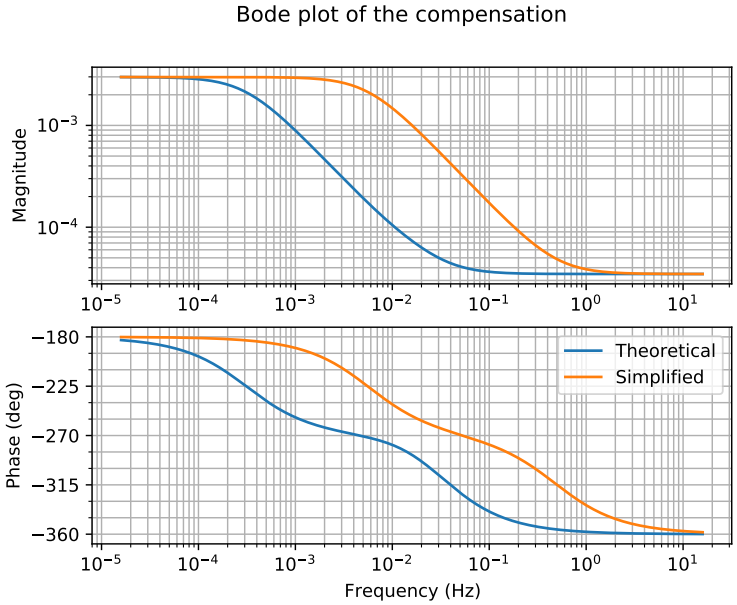

FIGURE 4.9: Bode diagram of the theoretical compensation equation in equation 4.11 and the simplified version in equation 4.13.

this substitution analytically, we find that the pole of the compensation function is

$$\omega_{pole} = \frac{K_{T,NTC}\alpha_{amb}\tau_{IPT}k_{IPT} - K_{T,NTC}\tau_{IPT}k_{IPT} + 2R_2\alpha_{amb} - R_2}{R_2\tau_{IPT}\left(2\alpha_{amb} - 1\right)} \tag{4.12}$$

This evaluates to 28.02 s in our case. We will start by setting the pole zero pair of the compensation at this value and correct for the assumption we made here during the experiments. The final simplified equation is

$$C_{ff,simplified} = \frac{C_{ff}(s=0) + \frac{C_{ff}(s\to\infty)}{\omega_{pole}}s}{1/\omega_{pole}s + 1} \tag{4.13}$$

and it's bode diagram can be seen in Figure 4.9. As it can be seen, the simplified equation is faster than the real compensation. This is because the pole of the peltier is not exactly compensated. We know that the final result will need a larger time constant than the one we calculated. As it can be seen, the simplified equation is faster than the real compensation. This is because the pole of the peltier is not exactly compensated. We know that the final result will need a larger time constant than the one we calculated.

Now, we have to implement this simplified system in an analog circuit. The circuit will have two branches, one low-pass and the other high-pass that correspond to the two responses and at the end they will be added together. This method enables us to create the desired response with a simple circuit. The system will be implemented with the circuit shown in Figure 4.10. First, there is a Wheatstone bridge to perform the first linearisation of the thermistor. The output of the bridge is taken by a differential operational amplifier that will find the difference between both branches. After this, there will be two branches for two different corrections, one for the residual compensation and another for the transient compensation. The first one will have a low pass filter whereas the second one will have a hight pass

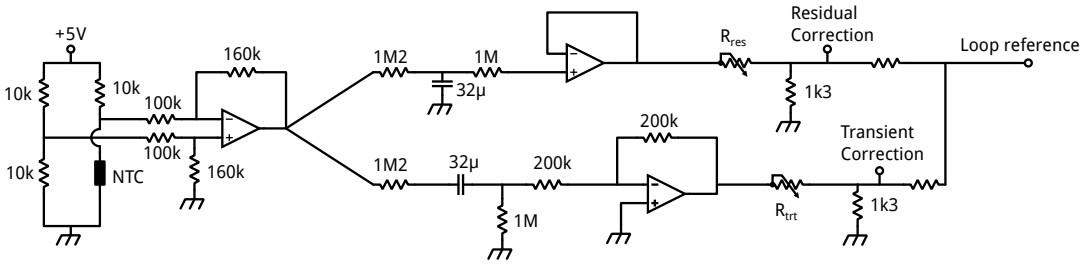

FIGURE 4.10: Compensation circuit implemented for the analog compensation.

filter, both filters will have the same cutoff frequency. After the filter, there is a gain stage that will modify the magnitude of each branch to the desired value depending on the correction it has to perform. There are two branches because the corrections have different sign.

We now have to calculate the values of R_{res} and R_{trt} to apply the desired correction. For the low-pass branch, we know that we have to correct $2.9 \cdot 10^{-3}$. We also know from the circuit, that the external thermistor will have a temperature sensitivity of 68 $mV/^{\circ}C$. From this, we can now find that the value of the resistance.

$$68\ mV/^{\circ}C \frac{1.3\ k\Omega}{R_{res} + 1.3\ k\Omega} = 2.9 \cdot 10^{-3}\ V/^{\circ}C \implies R_{res} = 30.88\ k\Omega \tag{4.14}$$

We apply the same method for the high-pass branch, now taking into account that the filter attenuates by 7 and we get $R_{trt} = 5.52\ k\Omega$.

Residual compensation

Now we will fine-tune the values obtained. First we focus on the residual compensation. The transient compensation branch is deactivated so the only effect is the residual one. Different tests are performed with different values of R_{res}. In these tests, the value of the potentiometer R_{res} has been changed. Each test was showing a smaller error for the residual part of the response. After these iterative tests, the final value of the potentiometer is $R_{res} = 45.93\ k\Omega$ and the resulting frequency variation can be seen in Figure 4.11. We can see that the frequency beat of the two lasers now reaches a steady state. The system was still stabilizing at the beginning of the test, that is why there is a small variation. After the jump in temperature, the difference in frequency is 50 GHz. This is small enough to start with the transient compensation. The value of R_{res} will still be changed to find the value for the zero frequency variation. The value that was reached for absolute compensation is $R_{res} = 42.51\ k\Omega$.

Transient compensation

With this, now we can see that the transient part of the response has increased in magnitude. This implies that the compensation has to be larger, and the potentiometer value smaller. Following the same technique as before by performing multiple tests changing the value of the potentiometer we reach the best value for the compensation. The result can be seen in Figure 4.12. As it can be seen, the compensation produces a peak before the transient response. This is because the time constant of the filter in the branch does not correspond to the time constant of the transient

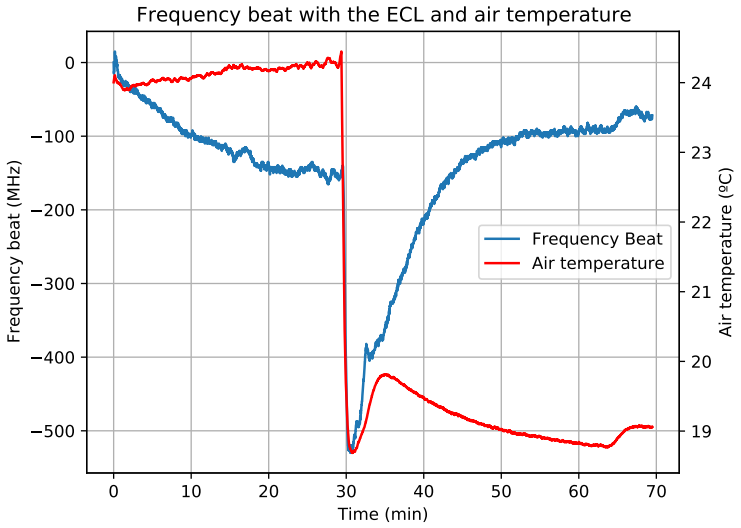

FIGURE 4.11: Frequency beat of the ECL and DFB when a step in air temperature is performed with the residual analog external thermistor compensation. Same setup as the other tests. The compensation comes from the variation of the loop reference. This is not the final compensation and the potentiometer has been further adjusted. The drift seen in this graph has been corrected on subsequent iterations.

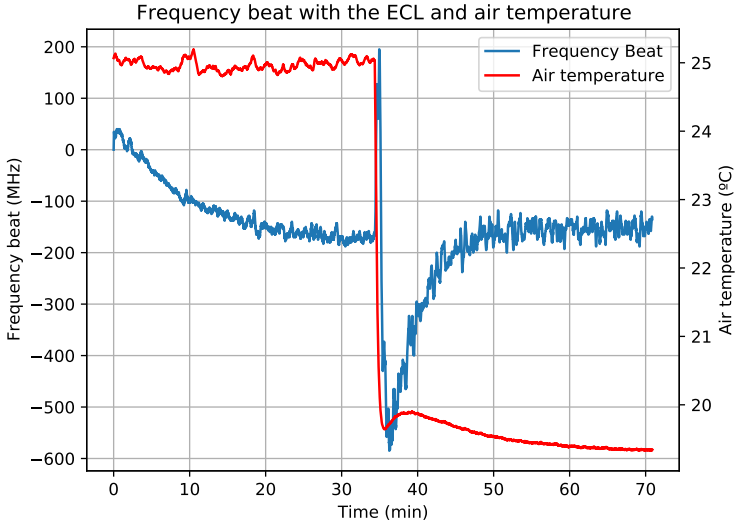

FIGURE 4.12: Frequency beat of the ECL and DFB when a step in air temperature is performed with the analog external thermistor compensation. Same setup as the other tests. The compensation comes from the variation of the loop reference.

response nor the bode diagram. In Figure 4.13, the voltage injected to the loop reference by the transient compensation branch can bee seen. The time to the steady state of this voltage is 8 minutes. The transient response takes 14 minutes to reach the steady state. The current capacitor is a 32 μF capacitor, so we can find that the needed capacitor is a 56 μF one. To extend the response, a 22 μF capacitor is soldered in parallel with the 32 μF one in the transient branch. In Figure 4.14 we can

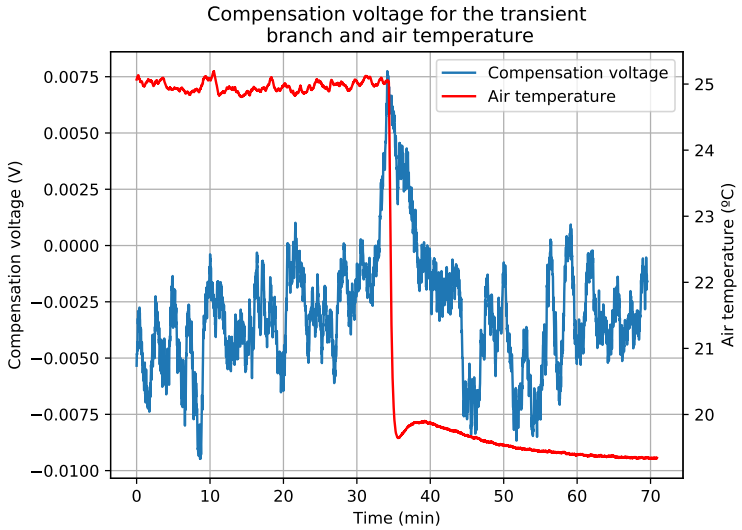

FIGURE 4.13: Voltage injected to the loop reference by the transient compensation. A moving mean of 100 samples has been applied to clean the output.

see the effect of different capacitances in the transient compensation branch. If the

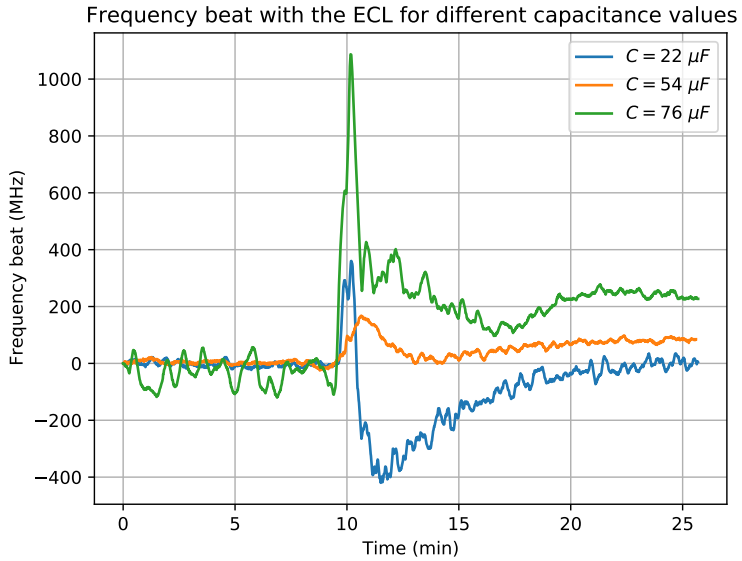

FIGURE 4.14: Frequency beat with the ECL for different capacitances in the transient branch. These capacitances make a filter with 200 $k\Omega$ resistors. The jump in temperature is the cooling jump in the other tests.

capacitor does not correspond to the transient response time, the compensation will not be effective. If it is too large, the compensation will take too much time to settle to a steady state and the response will be overcorrected. If it is to small, the compensation will settle too fast and the last part of the transient will not be corrected

Results

With the proper correction, the final result of the compensation is displayed in Figure 4.15. We can see that the residual compensation has been completely cancelled.

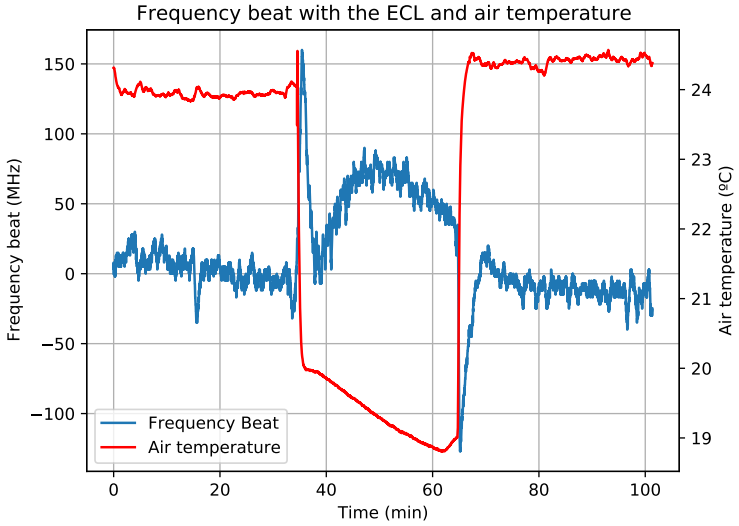

FIGURE 4.15: Frequency beat of the ECL and DFB when a step in air temperature is performed with the analog external thermistor compensation and the final values of the compensation. Same setup as the other tests. The compensation comes from the variation of the loop reference.

With the temperature changes of 5 $^{\circ}C$ the frequency drift is almost zero. For the transient part, there is still some variation. These peaks are $\pm 150\ MHz$ for this temperature change, this is $\pm 30\ MHz/^{\circ}C$. We have improved the stability of the system by almost ten times and reduced the time of the frequency drift. The peaks that appear on the frequency drift come from the higher order terms of the system. These are the best values we could find, the system will always experience the peaks shown in the graph. As we have created just a first order compensation, only the most dominant effect is cancelled. However, the peaks correspond to higher order responses of the laser. This higher order come from the simplification of the compensation function as well as the simplification of the laser model. This is the drawback of the analog compensation system. If a higher order has to be implemented, the complexity of the control will increase very rapidly. Also, these peaks appear when the jump is very sudden because they come from the high frequency parts of the response. If the temperature change is not as abrupt, the peaks disappear. In Figure 4.16 we can see the response with less abrupt temperature changes. We can see that with the compensation we have a stability of $\pm 200\ MHz$ for the 10 $^{\circ}C$ temperature change. This gives us a stability of 25 $MHz/^{\circ}C$. This is ten times better than with the simple PI controller. In the table 4.1 we can see the different improvements of each stage. We can see that with the static compensation (modifying R_{res}), the static error gets reduced and with the transient compensation the hole system is compensated.

We have also performed some tests for different capacitance values of the residual and transient branches. These tests can be seen in tables 4.3 and 4.2. In these tables, we can see the effects of the cut-off frequency of both filters. For the residual filter, we cannot see any effect on the compensation. This was expected as the filter for the residual branch is just to filter spurious signals that might come through

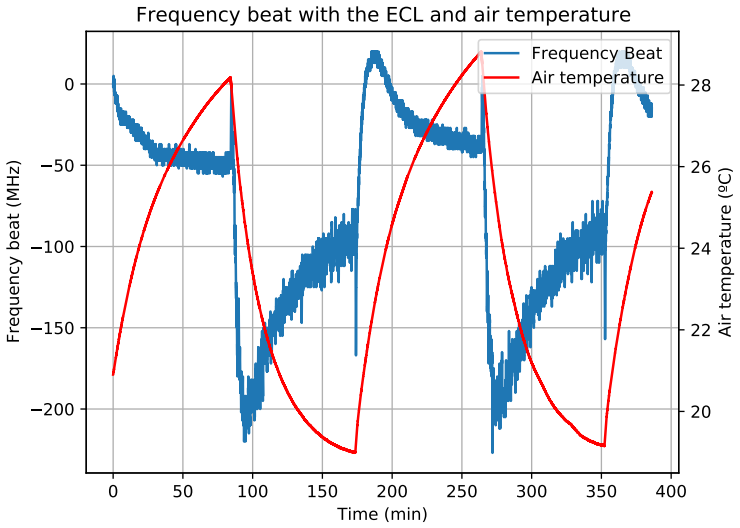

FIGURE 4.16: Frequency beat of the laser when the laser is inside the freezer and it cycles from on to off. The period is 3 hours and the temperature change is 10 *degreC*.

	R_{res}	C_{res}	τ_{res}	R_{trt}	C_{trt}	τ_{trt}	Static error $(MHz/°C)$	Peak to peak error $(MHz/°C)$
Original	∞	–	–	∞	–	–	206.875	225.625
Static compensation	45.17 $k\Omega$	32 μF	38.4 s	∞	–	–	12	80
Complete compensation	42.51 $k\Omega$	32 μF	38.4 s	1.029 $k\Omega$	54 μF	64.8 s	2	30

TABLE 4.1: Improvements from the original circuit, static compensation and complete compensation.

R_{res}	C_{res}	τ_{res}	R_{trt}	C_{trt}	τ_{trt}	Static error $(MHz/°C)$	Peak to peak error $(MHz/°C)$
45.17 $k\Omega$	32 μF	38.4 s	1.042 $k\Omega$	32 μF	38.4 s	1.67	58.33
41.68 $k\Omega$	32 μF	38.4 s	1.086 $k\Omega$	44 μF	52.8 s	8	60
42.51 $k\Omega$	32 μF	38.4 s	1.029 $k\Omega$	54 μF	64.8 s	2	30
42.51 $k\Omega$	32 μF	38.4 s	1.029 $k\Omega$	76 μF	91.2 s	40	220

TABLE 4.2: Different parameters of the compensation for different values of C_{trt}. There is a minimum in error at 54 μF. The values of the resistances change because the potentiometer was changed to a smaller value one and the system had to be readjusted, this changes are small and do not affect the stability.

that branch. The change in compensation regime from the transient to the residual is given by the cut-off frequency of the transient compensation. In this case, we can see a difference in the compensation. The main difference is in the peak to peak error. The residual error does not depend on this value so it is not affected. The results are the ones seen in Figure 4.14. If the pole does not mach the one on the system the compensation is too fast or slow. The fluctuations in the compensations for these tables are because the experiment is done by hand and the values of the resistances adjusted with a potentiometer and they change from experiment to experiment.

R_{res}	C_{res}	τ_{res}	R_{trt}	C_{trt}	τ_{trt}	Static error $(MHz/^{\circ}C)$	Peak to peak error $(MHz/^{\circ}C)$
42.51 $k\Omega$	0 μF	0 s	1.029 $k\Omega$	54 μF	64.8 s	19.6	58.82
41.68 $k\Omega$	10 μF	12 s	1.086 $k\Omega$	54 μF	64.8 s	10	50
42.51 $k\Omega$	32 μF	38.4 s	1.029 $k\Omega$	54 μF	64.8 s	2	30
42.51 $k\Omega$	54 μF	64.8 s	1.029 $k\Omega$	54 μF	64.8 s	12.5	87.5
41.68 $k\Omega$	76 μF	91.2 s	1.086 $k\Omega$	54 μF	64.8 s	10	30

TABLE 4.3: Different parameters of the compensation for different values of C_{res}. There is a no correlation between this value and the compensation error. The values of the resistances change because the potentiometer was changed to a smaller value one and the system had to be readjusted, this changes are small and do not affect the stability.

With this compensation scheme we have few parameters to control. We have R_{res} to control how much residual compensation is applied and it should be tuned until the residual error is zero. The R_{trt} controls how much transient compensation is applied (how high is the compensation peak), it should be tuned to cancel the initial jump in conjunction with C_{trt}. And we have C_{trt} to control the duration of the transient compensation, it should be tuned to mach the duration of the initial jump of the system. All in all, we can say we have found the best compensation possible with this system.

Chapter 5

Conclusions

After the analysis performed and the results obtained, there are some conclusions that follow. The complete analysis could be followed to implement a more accurate and robust control for the system. The complete model has much more parameters that the ones that were found in this work. The difference would be that all the parameters have a relation to physical properties of the laser construction and components. For example, all the thermal resistances have a direct relation to the thermal conductivity and contact area between the components and the capacitances have a relation with the mass and the specific heat capacitance. If this model where to be implemented, it would need a method of extracting all the parameters in the complete model.

The reduction of the model performed is similar to the real system. The measurements are consistent with the model and the parameter extraction matches the behaviour of the real laser. With this simplified model, the control system created also matches the behaviour of the real laser from the tests performed.

The original control system can be improved with various modifications. The complexity can be increased. If a more complex control system is used, the tuning can be faster and with less error. A more complex system would be difficult to implement with an analog circuit so the next step should be to change the control to a digital scheme. If a digital system is implemented, the non linearities can also be compensated. The control can convert the voltage to the real temperature measured by the thermistor using the complete thermistor equation and no linearisation needs to be performed. Also, a non-linear control or an adaptative controller could be implemented. Using machine learning, with a system that is well-defined, an adaptative controller can be much more robust against bigger changes. As this system is dealing with non linearities from multiple sources, it could compensate for the lack of simple equations to describe the system.

Even with the improved control, there is the problem of the laser chip temperature difference with the thermistor temperature. The modified control proposed aims to solve this problem. The feed-forward system increases complexity of the system but the results are much better than the simple system. The implementation with the digital system has some problems as it has been pointed out. With a better implementation it could have similar results as the analog implementation. It would also be more flexible, so it would be easier to implement on other lasers given that there is huge variability. The results on the analog compensation scheme exceed our expectations. A system with such stability in front of temperature changes could be implemented without a problem and would probably outperform the current system.

From this analysis it can be concluded that the lasers studied are very complex systems. The effort to simplify these systems has been a noble, the simplified system is close to the real component behaviour and the parameter extraction experiments

correspond with what was expected. As it is a very complex system, not all the interactions are modelled with such a simplified model and some difference between the model and the real world exists. The implementation of such a simple control scheme, even with the improvements in wavelength stability with temperature, has some performance issues. However, these can be resolved with the solutions proposed or by implementing a more complex feed-forward control scheme to have a very stable system that is robust against temperature changes. Even without the accurate model, the parameters for the control system and stabilization have been found and the laser stabilized in front of temperature variations.

Appendix A

Final equation

This is the resulting equation after combining all 21 Kirchhoff equations.

$$\frac{T_L(s)}{\mathrm{Q_l}(s)} = -\frac{R_L\left(C_h R_{carr} R_p s + R_{carr} + R_p\right)}{-C_L C_h R_L R_{carr} R_p s^2 + R_{carr} + R_p + s\left(C_L R_L R_{carr} + C_L R_L R_p + C_h R_{carr} R_p\right)} \tag{A.1}$$

$$\frac{T_L(s)}{\mathrm{Q_p}(s)} = \frac{R_{SM} R_p}{-C_L C_h R_L R_{carr} R_p s^2 + R_{carr} + R_p + s\left(C_L R_L R_{carr} + C_L R_L R_p + C_h R_{carr} R_p\right)} \tag{A.2}$$

$$\frac{T_L(s)}{\mathrm{T_p}(s)} = \frac{R_{SM}}{-C_L C_h R_L R_{carr} R_p s^2 + R_{carr} + R_p + s\left(C_L R_L R_{carr} + C_L R_L R_p + C_h R_{carr} R_p\right)} \tag{A.3}$$

$$\frac{T_L(s)}{\mathrm{T_a}(s)} = -\frac{R_{SM}\left(C_h R_{carr} R_p s - R_{carra} + R_{carr} + R_p\right)}{R_{carra}\left(-C_L C_h R_L R_{carr} R_p s^2 + R_{carr} + R_p + s\left(C_L R_L R_{carr} + C_L R_L R_p + C_h R_{carr} R_p\right)\right)} \tag{A.4}$$

$$
\begin{aligned}
\frac{T_L(s)}{\mathrm{T_{ntc}}(s)} =& \frac{-C_h C_{NTC} C_{carr} R_{NTC} R_{SM} R_{carra} R_{carr} R_p s^3}{R_{carra}\left(-C_L C_h R_L R_{carr} R_p s^2 + R_{carr} + R_p + s\left(C_L R_L R_{carr} + C_L R_L R_p + C_h R_{carr} R_p\right)\right)} \\
& s^2\Bigg(\frac{\left(-C_h C_{NTC} R_{NTC} R_{SM} R_{carra} R_p + C_h C_{NTC} R_{NTC} R_{SM} R_{carr} R_p\right.}{R_{carra}\left(-C_L C_h R_L R_{carr} R_p s^2 + R_{carr} + R_p + s\left(C_L R_L R_{carr} + C_L R_L R_p + C_h R_{carr} R_p\right)\right)} \\
& + \frac{-C_h R_{carra} R_{carr} R_p \left(C_{NTC} R_{NTC} + C_{NTC} R_{SM} + C_{carr} R_{SM}\right) - C_{NTC} C_{carr} R_{NTC} R_{SM} R_{carra} R_{carr}}{R_{carra}\left(-C_L C_h R_L R_{carr} R_p s^2 + R_{carr} + R_p + s\left(C_L R_L R_{carr} + C_L R_L R_p + C_h R_{carr} R_p\right)\right)} + \\
& \frac{\left.-C_{NTC} C_{carr} R_{NTC} R_{SM} R_{carra} R_p\right)}{R_{carra}\left(-C_L C_h R_L R_{carr} R_p s^2 + R_{carr} + R_p + s\left(C_L R_L R_{carr} + C_L R_L R_p + C_h R_{carr} R_p\right)\right)}\Bigg) \\
& - s\Bigg(\frac{\left(C_h R_{SM} R_{carra} R_p - C_h R_{SM} R_{carr} R_p + C_h R_{carra} R_{carr} R_p + C_{NTC} R_{NTC} R_{SM} R_{carra}\right.}{R_{carra}\left(-C_L C_h R_L R_{carr} R_p s^2 + R_{carr} + R_p + s\left(C_L R_L R_{carr} + C_L R_L R_p + C_h R_{carr} R_p\right)\right)} + \\
& \frac{-C_{NTC} R_{NTC} R_{SM} R_{carr} - C_{NTC} R_{NTC} R_{SM} R_p + R_{carra} R_{carr}\left(C_{NTC} R_{NTC} + C_{NTC} R_{SM} + C_{carr} R_{SM}\right)}{R_{carra}\left(-C_L C_h R_L R_{carr} R_p s^2 + R_{carr} + R_p + s\left(C_L R_L R_{carr} + C_L R_L R_p + C_h R_{carr} R_p\right)\right)} + \\
& \frac{\left.R_{carra} R_p \left(C_{NTC} R_{NTC} + C_{NTC} R_{SM} + C_{carr} R_{SM}\right)\right)}{R_{carra}\left(-C_L C_h R_L R_{carr} R_p s^2 + R_{carr} + R_p + s\left(C_L R_L R_{carr} + C_L R_L R_p + C_h R_{carr} R_p\right)\right)}\Bigg) + \\
& \frac{-R_{SM} R_{carra} + R_{SM} R_{carr} + R_{SM} R_p - R_{carra} R_{carr} - R_{carra} R_p}{R_{carra}\left(-C_L C_h R_L R_{carr} R_p s^2 + R_{carr} + R_p + s\left(C_L R_L R_{carr} + C_L R_L R_p + C_h R_{carr} R_p\right)\right)}
\end{aligned}
\tag{A.5}
$$

These equations have been separated for better interpretation, the complete equation should be

$$
T_L(s) = \frac{T_L(s)}{\mathrm{Q_p}(s)}\,\mathrm{Q_p}(s) + \frac{T_L(s)}{\mathrm{Q_p}(s)}\,\mathrm{Q_p}(s) + \frac{T_L(s)}{\mathrm{T_p}(s)}\,\mathrm{T_p}(s) + \frac{T_L(s)}{\mathrm{T_a}(s)}\,\mathrm{T_a}(s) + \frac{T_L(s)}{\mathrm{T_{ntc}}(s)}\,\mathrm{T_{ntc}}(s) \tag{A.6}
$$

Bibliography

[1] ITU-T Telecommunication standardization sector of itu, "Gigabit-capable passive optical networks (GPON): General characteristics," en, Telecommunication standardization sector of itu, Geneva, CH, Standard ITU-T/UIT-T G.984.1 (03/08), 2008. [Online]. Available: https://www.itu.int/rec/T-REC-G.984.1.

[2] ——, "Gigabit-capable passive optical networks (GPON): Physical media dependent (PMD) layer specification," en, Telecommunication standardization sector of itu, Geneva, CH, Standard ITU-T/UIT-T G.984.2 (08/19), 2019. [Online]. Available: https://www.itu.int/rec/T-REC-G.984.2.

[3] ——, "40-Gigabit-capable passive optical networks 2 (NG-PON2): Physical media dependent (PMD) layer specification," en, Telecommunication standardization sector of itu, Geneva, CH, Standard ITU-T/UIT-T G.989.2 (02/19), 2019. [Online]. Available: https://www.itu.int/rec/T-REC-G.989.2.

[4] V. Sales, J. Segarra, V. Polo, J. C. Velásquez, and J. Prat, "Udwdm-pon using low-cost coherent transceivers with limited tunability and heuristic dwa," *IEEE/OSA Journal of Optical Communications and Networking*, vol. 8, no. 8, pp. 582–599, 2016. DOI: 10.1364/JOCN.8.000582.

[5] Y. Sheikhnejad, R. Bastos, Z. Vujicic, A. Shahpari, and A. Teixeira, "Laser thermal tuning by transient analytical analysis of peltier device," *IEEE Photonics Journal*, vol. 9, no. 3, pp. 1–13, 2017. DOI: 10.1109/JPHOT.2017.2695522.

[6] H. Wang and Y. Yu, "New theoretical model to analyze temperature distribution and influence of thermal transients of an sg-dbr laser," *IEEE Journal of Quantum Electronics*, vol. 48, no. 2, pp. 107–113, 2011.

[7] M. Jaegle *et al.*, "Multiphysics simulation of thermoelectric systems-modeling of peltier-cooling and thermoelectric generation," in *COMSOL Conference 2008 Hannover*, 2008.

[8] G. Mulvihill and R. O'Dowd, "Thermal transient measurement, modeling, and compensation of a widely tunable laser for an optically switched network," *Journal of lightwave technology*, vol. 23, no. 12, p. 4101, 2005.

[9] J.-H. Meng, X.-D. Wang, and X.-X. Zhang, "Transient modeling and dynamic characteristics of thermoelectric cooler," *Applied energy*, vol. 108, pp. 340–348, 2013.

[10] R. C. Steere, "Solution of two dimensional transient heat flow problems by electrical analogue," *Physics Education*, vol. 6, no. 6, pp. 443–447, 1971. DOI: 10.1088/0031-9120/6/6/006. [Online]. Available: https://doi.org/10.1088/0031-9120/6/6/006.

[11] S. Lineykin and S. Ben-Yaakov, "Pspice-compatible equivalent circuit of thermoelectric cooler," in *2005 IEEE 36th Power Electronics Specialists Conference*, 2005, pp. 608–612. DOI: 10.1109/PESC.2005.1581688.